Radiocarbon evidence of a North Atlantic intermediate water reconfiguration between the 1960s and 1980s

Qian Liu [a,b*], Laura F. Robinson [b, c], Erica Hendy [b], Joseph A. Stewart [b], Tao Li [a], Tianyu Chen [d], Timothy D. J. Knowles [e]

[a] State Key Laboratory of Palaeobiology and Stratigraphy, Nanjing Institute of Geology and Palaeontology, Chinese Academy of Sciences, Nanjing, China.

[b] School of Earth Sciences, University of Bristol, Bristol, UK.

[c] Department of Environment and Geography, University of York, York, UK.

[d] State Key Laboratory for Mineral Deposits Research, School of Earth Sciences and Engineering and Frontiers Science Center for Critical Earth Material Cycling, Nanjing University, Nanjing, China.

[e] Bristol Radiocarbon Accelerator Mass Spectrometry, University of Bristol, Bristol, UK.

[*]Corresponding author: Qian Liu (qianliu@nigpas.ac.cn; lqian.526@gmail.com)

Abstract

The Atlantic Meridional Overturning Circulation (AMOC) is a critical modulating component of the Earth's climate system, therefore, documenting the timing and amplitude of AMOC variability since the Industrial Era is essential for understanding future climate. However, there are very few continuous high-resolution records from this time period in the subsurface ocean which restricts us from exploring the nature of changes in the ocean interior. Here, we present

new seawater radiocarbon (^{14}C) records of intermediate depth water (between 1400 m and 2000 m) for the Industrial Era since 1830 CE obtained from the calcitic skeleton of four cold-water bamboo corals from the tropical Atlantic. These samples were collected in 2013 with lifespans ranging from 64 to 161 years. No bomb ^{14}C was detected in the calcitic skeleton, indicating that the tropical intermediate North Atlantic had not yet been invaded by bomb ^{14}C at the time of collection. The data show a relatively constant $\Delta^{14}C$ before 1960 CE with a synchronous basin-wide increase in ^{14}C content reached by 1980 CE. The stepwise shift in $\Delta^{14}C$ may be explained by the North Atlantic Deep Water (NADW) becoming shallower in the tropical North Atlantic and/or a southward retreat of Antarctic Intermediate Water (AAIW), in either case potentially linked to a weakening of AMOC. Our study indicates synchronous large-scale oceanic reconfiguration occurred throughout the tropical and North Atlantic starting in the 1960s and that there has been no subsequent return to the state of the pre-mid-20th century oceanic interior.

Key words: Atlantic Meridional Overturning Circulation (AMOC), Cold-water corals (CWCs), Radiocarbon, Bomb radiocarbon, Tropical Atlantic, North Atlantic Deep Water (NADW), Antarctic Intermediate Water (AAIW)

Highlights:

- Tropical North Atlantic intermediate water $\Delta^{14}C$ increased by ~9 ‰ between the 1960s and 1980s.
- No bomb ^{14}C recorded in coral calcitic skeletons when they were collected in 2013.
- Tropical NADW may have become shallower and/or AAIW have retreated after the 1960s.

1. Introduction

Atlantic Meridional Overturning Circulation (AMOC) is one of the major ocean circulation systems. It transports heat, carbon and nutrients across the Equator to the North, so any changes in the AMOC have the potential to disrupt regional and global climate and productivity patterns (Broecker, 1991; Hu et al., 2020; Liu et al., 2020; Lynch-Stieglitz et al., 2024; Schmittner, 2005). Although the exact timing and extent of weakening continue to be debated (Kilbourne et al., 2022; Rahmstorf, 2024; van Westen et al., 2024), recent studies suggest that AMOC has weakened over the last century, with growing evidence for a marked change in the 1970s (Caesar et al., 2021; Rahmstorf et al., 2015; Thornalley et al., 2018). However, variations in the associated water masses, particularly in the tropical Atlantic, remain largely unknown, as most model and proxy records are concentrated in the polar regions. Consequently, the implications of a rapidly weakening AMOC on the transport of heat, carbon, and nutrients on decadal timescales are unclear, thus complicating predictions of future climate and productivity patterns. Therefore, understanding the variations in water masses is critical to forecasting future climate changes and their potential impacts.

The shallow to deep circulation of the AMOC comprises North Atlantic deep water (NADW) and Antarctic intermediate water (AAIW) which are both influenced by AMOC strength, but the details of how they respond to changes in AMOC remain an active area of research (Gu et al., 2017; Huang et al., 2014; Pahnke et al., 2008). In addition, a slowdown of AMOC would lead to a deepening of the tropical Atlantic thermocline (Pedro et al., 2018; Stewart et al., 2023; Timmermann et al., 2005). The subtropical/tropical Atlantic thermocline is mainly filled with North Atlantic Central Water (NACW) above South Atlantic Central Water (SACW) and modified AAIW below (mAAIW; a mixture of AAIW and Upper Circumpolar Deep Water) (Bub and Brown, 1996; Huang et al., 2012; Jenkins et al., 2015; Poole and Tomczak, 1999). In

a weakened AMOC state, the NACW and SACW potentially move southward (Huang et al., 2012) as well as AAIW.

Given the importance of AMOC to global heat transportation, reconstruction of recent Atlantic water mass variations and their linkages to climate change is vital. In this study, we compare coral, seawater and modelling radiocarbon (^{14}C) data to explore the potential reconfigurations of water masses in the tropical Atlantic interior over the last century.

Natural ^{14}C is produced in the atmosphere by cosmogenic rays and invades the surface ocean by air-sea exchange (Broecker et al., 1960). The atmospheric-sourced ^{14}C in the ocean and its known decay rate make it a powerful tracer for ocean circulation and ventilation as well as water-mass mixing (Adkins et al., 1998; Burke and Robinson, 2012; Graven et al., 2012; Lower-Spies et al., 2020; Rafter et al., 2022; Skinner and Bard, 2022). NADW and AAIW have distinct $\Delta^{14}C$ based on their sources and ventilation rates (for modern seawater, $\Delta^{14}C = (Fm \times \exp(-t/8267) - 1) \times 1000$, where Fm is the fraction modern of the sample and t is years elapsed from 1950 CE until the year of the sample measurement). NADW is a relatively young deep water mass, sourced from northern North Atlantic surface water, and has a typical $\Delta^{14}C$ of -86 ± 8‰ in the tropical Atlantic (Broecker et al., 1960; Kromer, 2014; Olsen et al., 2020, 2019). By contrast, AAIW is more depleted in radiocarbon given lower rates of air-sea gas exchange in the Antarctic, as well as a longer transit time to the tropical Atlantic (Fu et al., 2018) and has a typical $\Delta^{14}C$ of -99 ± 11‰ (Broecker et al., 1960; Kromer, 2014; Olsen et al., 2020, 2019) in the tropical North Atlantic. The depth profile of $\Delta^{14}C$ in the Atlantic therefore varies depending on water masses present at any specific location (Figure 1).

In addition to natural variations in ^{14}C, large amounts of ^{14}C were generated in the atmosphere from the testing of nuclear weapons in the 1950s and 1960s. The atmospheric bomb ^{14}C evolution curve clearly shows the start of bomb ^{14}C increase at around 1955 CE, rapidly

reaching a maximum at around 1965 CE in the Northern Hemisphere (Hua et al., 2013) before abruptly decreasing again, in part, due to the influence of ^{14}C-free fossil fuel burning (i.e., the Suess Effect) and air-sea exchange (Graven, 2015; Graven et al., 2012). This bomb ^{14}C provides a useful tracer of ocean surface-to-deep transportation over the last century (Broecker et al., 1978; Grammer et al., 2015; Graven et al., 2012). Bomb ^{14}C in the North Atlantic surface ocean started to accumulate in ~1957 CE (Druffel, 2002; Druffel, 1989) and reached a maximum between the 1970s and 1990s depending on location, depth, and oceanographic setting (Druffel, 2002; Fernandez et al., 2015; Liu et al., 2023). For example, in the northwest Atlantic surface ocean, the maximum bomb ^{14}C occurred around 1983 CE as recorded in the organic skeleton of a gorgonian coral *Primnoa resedaeformis* collected in the Hudson Strait (Sherwood et al., 2008), which is ~10 years later and more than 100‰ depleted than the western subtropical Atlantic surface ocean due to deep mixing (Azetsu-Scott et al., 2005; Druffel, 1980). The temporal evolution of the bomb ^{14}C curve therefore provides a way to determine the timescales of deep ocean circulation (Jenkins et al., 2015).

A valuable archive of ^{14}C is cold-water corals (CWCs), in particular bamboo corals that create robust organic and calcitic skeletons, which can be used to construct continuous high-resolution records of past ocean environments as mentioned above (Farmer et al., 2015a; Geyman et al., 2019; Sherwood et al., 2008). Bamboo corals are so named because of their distinct bamboo-like morphology that includes a jointed skeleton with dark proteinaceous organic nodes separating high-Mg calcitic internodes (Noé and Dullo, 2006; Roark et al., 2005). The two components of the coral skeleton grow concentrically and synchronously (Noé and Dullo, 2006), providing temporally-linked geochemical records from both organic and calcitic components.

The organic node of bamboo corals is annually banded so that organic node band-counting

methods can be used to develop age models for bamboo corals (Sherwood and Edinger, 2009). Correspondingly, the age model of the calcitic section can be determined by comparison to the growth rate derived from organic node band-counting (Liu et al., 2023; Noé and Dullo, 2006). This ^{14}C independent age model makes bamboo corals a valuable archive of ocean interior ^{14}C variation in the past. Moreover, the calcitic skeleton of bamboo corals is formed from ambient seawater, and thus records seawater conditions at the time of coral growth. For example, the Ba/Ca ratio of the bamboo coral calcitic skeleton has been explored as a proxy of seawater Ba concentration (Geyman et al., 2019; LaVigne et al., 2011; Serrato Marks et al., 2017). In addition, $\Delta^{14}C$ recorded in the calcitic part of bamboo corals has been used to reconstruct the $\Delta^{14}C$ variation of deep seawater (Farmer et al., 2015b; Sherwood et al., 2008).

Here we present ^{14}C records recorded in the calcitic skeleton of four bamboo corals collected from the central and eastern tropical Atlantic around 1400 m and 2000 m water depths in 2013 CE. With growth rates generated by band counting of the organic nodes (Liu et al., 2023), this study uses age models for calcitic coral sections which do not rely on radiocarbon dating, permitting the use of ^{14}C measurements as a tracer for circulation change. The coral ages date back to the 1800s, therefore allowing us to reconstruct water masses exchange variation of tropical Atlantic since the Industrial Era.

2. Methodology

2.1. Coral samples

The four bamboo corals used in this study were collected by remotely operated vehicle (ROV) during the RRS James Cook expedition JC094 in October 2013 (Robinson, 2014) and are from the eastern and central tropical North Atlantic Ocean at 1400 m to 2000 m water depth (Figure 1; Table 1). Specifically, two corals were collected from the Carter and Knipovich Seamounts in the east and two corals from the Vema Fracture Zone and Vayda Seamount in the central tropical North Atlantic Ocean. Each coral was named by a simplified identifier notation that includes the abbreviated location name and water depth information (e.g., Car_1409m for the coral collected from Carter Seamount at 1409 m).

2.2. Oceanographic Setting

The 1400 m to 2000 m depth range where the four bamboo corals were collected is filled by northward mAAIW and a deeper southward NADW (Figure 1; (Emery and Meincke, 1986; Talley et al., 2011)). The mAAIW is distributed between 500 m and 1500 m depth across most of the Atlantic Ocean up to ~20°N with a decreasing trend of water mass fraction and depth towards the north (Kirchner et al., 2009; Talley, 1996). Above mAAIW is the thermocline water which includes NACW and SACW (Poole and Tomczak, 1999). SACW is distributed up to 800 m water depth and deviates as far northwards as 20°N (Poole and Tomczak, 1999; Stramma and Schott, 1999). Below mAAIW is NADW which is distributed between 1500 m and 4000 m (Jenkins et al., 2015).

2.3. Analytical techniques

2.3.1 Sample preparation

Each calcitic radial section was cut below the basal organic node of each coral for approximately 1 cm slice using an IsoMet® low speed saw (Buehler). The polished coral slice was photographed under a reflected light microscope camera with its radius measured. Powder subsamples were then milled out radially with 0.2 to 0.5 mm resolution using a micro-mill (New Wave Research) with ø1 mm flat end mill bit (Komet). The slice was rinsed and ultrasonicated in Milli-Q water between each drilling and photographed to measure the longest radius so that the interval of each subsample could be determined.

2.3.2 Cleaning procedure

Powdered subsamples were oxidatively cleaned with 1:1 30% H_2O_2 and 1N NaOH to remove any organic matter following the procedure of Adkins et al. (2002). About 15 mg of each powdered subsample was weighed into acid cleaned glass vials and 5 mg was leached away by 0.05N HCl immediately before the remainder of the sample was analysed for radiocarbon content (Adkins et al., 2002). The powdered subsample was dried on a 60 ℃ hotplate and weighed before being graphitized.

2.3.3 Radiocarbon measurement

The powdered subsamples were measured at the Bristol Radiocarbon Accelerator Mass Spectrometry (BRAMS) Facility at the University of Bristol following the procedure of Knowles et al. (2019). The calcitic powder samples were graphitized using an IonPlus automatic graphitization equipment (AGE3) system. The graphite targets pressed by an IonPlus PSP were measured for radiocarbon on the BrisMICADAS which is a compact 200kV

MICADAS AMS.

2.3.4 Radiocarbon calculation

Radiocarbon data were originally provided as blank-corrected fraction modern (F_m) which is the δ^{13}C-normalized ratio between the measured sample $^{14}C/^{12}C$ and the $^{14}C/^{12}C$ of NBS Oxalic Acid II at 1950 CE. $D^{14}C$ (‰; age uncorrected) were calculated using Equation 1. $\Delta^{14}C$ (‰; age corrected) were calculated using Equation 2 (Stuiver and Polach, 1977).

$$D^{14}C\ (‰) = (F_m - 1)*1000 \qquad \text{Equation 1}$$

$$\Delta^{14}C\ (‰) = \left[F_m * e^{\lambda(1950-Y_c)} - 1\right] * 1000 \qquad \text{Equation 2}$$

Where Yc is the coral skeleton formation year derived from age models calculated in Section 2.4, λ is the reciprocal of the true mean ^{14}C life (8267 years, (Godwin, 1962)). $\Delta^{14}C$ allows direct comparison of radiocarbon content in samples from different ages by accounting for radiocarbon decay occurring between the time of sample formation and radiocarbon analysis.

2.4. Age model development

The age models of the four corals were developed in Liu et al. (2023) for the organic nodes. Given synchronous growth in the radial direction (Noé and Dullo, 2006), calcitic radial sections share the same relative age as their organic node. The longest-lived coral is Vem_1474m which was dated back to 1831 CE and the youngest, Car_1409m, dated back to 1950 CE (Table 1). The time range over each calcitic subsample was formed is listed in Table S1.

The radii of the organic node and calcitic section are different, so that the growth rates of the organic node subsamples cannot be applied to calcitic sections directly (Table 1). Instead, a linear growth rate for each subsample of organic node was calculated using the distance of the

subsample interval and the average counted layers (Liu et al., 2023). After matching the calcitic section and organic node subsamples based on their distances from the outer edge (calcitic section distance × ratio between radius of organic node and calcitic section), the growth rates were applied to the matched calcitic section subsamples (Table S1). The collection date (decimal year 2013.8) was assigned to the outermost edge of each calcitic section for Car_1409m and Vay_1455m. However, it has already been shown that the other two corals stopped growing before collection (Kni_1985m and Vem_1474m), therefore, the calculated year of each coral edge based on its organic node was applied, 1987 CE and 1992 CE for Kni_1985m and Vem_1474m, respectively (Table 1;(Liu et al., 2023)).

2.5. Comparative $\Delta^{14}C$ data compilation

2.5.1 Seawater dissolved inorganic carbon (DIC) $\Delta^{14}C$ data

To put our coral ^{14}C data into context, observed seawater $\Delta^{14}C$ profiles were collated for comparison (Table S2; Figure 2). Seventeen profiles were collated from 1973 CE to 2013 CE in which nine profiles were sourced from GLODAPv2021 (Kromer, 2014; Olsen et al., 2020, 2019) and eight profiles were sourced from JC094 cruise data (Chen et al., 2015). The cruise data are divided by CTD and ROV, in which CTD collected water samples away from the seamounts to reach the seafloor while ROV collected water samples on the seamounts slope where the corals were collected (Robinson, 2014). Therefore, the ROV data should be the closest possible match to the seawater $\Delta^{14}C$ at our coral sites. Seawater data were divided by location near Vem_1474m, Vay_1455m, Car_1409m, and Kni_1985mas indicated by colour code (Figure 1b, c).

2.5.2 Earth-System-Model-derived $\Delta^{14}C$ outputs

In addition to observed seawater data, climate model outputs were compiled to compare with

our coral ^{14}C data. The historical simulation of all three models (CESM2, CESM2-FV2, MRI-ESM2-0) incorporated ^{14}C within Coupled Model Intercomparison Project Phase 6 (CMIP6) were compiled. All 15 ensembles outputs were extracted and compiled, including 11 ensembles in CESM2, 3 in CESM2-FV2 and 1 in MRI-ESM2-0. Model outputs of abiotic dissolved inorganic total carbon ('dissicabio') and abiotic dissolved inorganic carbon-14 ('dissi14cabio') concentration (Danabasoglu, 2019; Orr et al., 2017) were used to calculate modelled seawater $\Delta^{14}C$ using the following equation (Orr et al., 2017):

$$\Delta^{14}C = (\text{dissi14cabio}/\text{dissicabio} - 1) \times 1000 \quad \text{Equation 3}$$

for the period 1900 CE to 2014 CE at depths proximal to each coral collection site. The model outputs have been normalized by $\delta^{13}C$ and the calculated $\Delta^{14}C$ can be compared directly with measured data (Orr et al., 2017). The modelled seawater $\Delta^{14}C$ of North Atlantic at 1500 m and section profile in 2010 CE were also calculated (Figure 1a, d).

The comparisons between each ensemble outputs and coral ^{14}C are shown in Figure A1. Despite absolute value offsets existing between model runs (less than 5‰ in our coral locations), the general trends and timings agree with each other in model CESM2 and CESM2-FV2 (Figure A1). There are limited differences between each ensemble within each model. However, ^{14}C variations in model MRI-ESM2-0 show distinct differences from the other two models and different from observations. Therefore, we did not include MRI-ESM2-0 outputs in our coral-model comparison. In light of the better agreement between Northwest Atlantic surface coral and model simulations (Figure A1b), we chose the average result of all 11 ensembles in historical simulations of CESM2 in our discussion.

3. Results and Discussion

3.1 Seawater DIC $\Delta^{14}C$ reconstructed from bamboo coral calcitic $\Delta^{14}C$

Overall, the $\Delta^{14}C$ recorded in the calcite sections of the four bamboo corals is consistent with the relevant seawater $\Delta^{14}C$ profiles (Figure 2; Figure 3), confirming that bamboo coral calcite records ambient seawater $\Delta^{14}C$.

There are generally two stages of $\Delta^{14}C$ recorded in all four corals. The $\Delta^{14}C$ before 1960 CE is lower and constant, averaging -89 ± 2‰ (n = 13, 1SD). After 1960s, the $\Delta^{14}C$ increases to -81 ± 4‰ in 1980s in both central and eastern sites and remains this way in both Vay_1455m and Car_1409m (Figure 3). The detailed comparations of coral $\Delta^{14}C$ with seawater observations and model results in central and eastern Atlantic are discussed below.

3.1.1 Central Atlantic Sites

The two central Atlantic corals were collected from around 1500 m depth, within the transition layer between mAAIW and NADW (Figure 1d). Given the large difference in $\Delta^{14}C$ between these water masses (-99 ± 11‰ and -86 ± 8‰, respectively) (Broecker et al., 1960; Kromer, 2014; Olsen et al., 2020, 2019), small changes in circulation may have a relatively large impact on seawater (or coral) $\Delta^{14}C$.

The most obvious difference between the coral and seawater data is in the most modern samples (2013 CE). Seawater data show $\Delta^{14}C$ values up to -59‰ which is 21‰ higher than the coral data (Figure 3a). We interpret this seawater data as invasion of bomb radiocarbon, which is not yet seen in the accumulated coral carbonate. In support of the invasion of bomb radiocarbon into the ocean, there is a significant increase of $\Delta^{14}C$ (by ~40 ‰) between 1983 CE and 2013 CE in NADW at a location 3 degrees to the west of Vay_1455m (GRM as shown in Figure 1b;

Figure 2a). The comparison between significant enrichment of ^{14}C in GRM and slight enrichment of ^{14}C in the central Atlantic suggests that bomb ^{14}C had not started influencing the coral collection sites until 2013 CE. That explains the discrepancy between seawater and coral data in 2013 CE as the bomb signal cannot yet be resolved by our coral sampling technique.

Prior to the most recent seawater data in 2013 CE, $\Delta^{14}C$ in the corals are very similar to seawater. At Vay_1455m the coral $\Delta^{14}C$ is constant at -90‰, then jumps up by 9‰ to -81‰ at 1979 CE (Figure 3a). Local seawater data are closely aligned with these data, supporting the coral-based step change. The $\Delta^{14}C$ in coral Vem_1474m shows a remarkably similar step change in the 1960s from consistent values of -91‰ towards higher values of -83‰. There are only 3 seawater profiles very close to Vem_1474m, two from the 1980s and one in 2013 CE. The 1980s seawater $\Delta^{14}C$ data are ~11‰ lower than the corals (Figure 3a). However, this mismatch is not surprising, as the seawater samples were collected from the northeast where the $\Delta^{14}C$ is lower than the coral location in the modern day (Figure 1a, b).

3.1.2 Eastern Atlantic Sites

In the east, there is more variability in both the coral and seawater data (Figure 3b). Car_1409m sits towards the top of NADW, whilst Kni_1985m is located below it, within modern NADW. This variability is expected, given the difference in oceanographic setting and the locations of both corals in water mass transition zones (Figure 2b).

Seawater $\Delta^{14}C$ in 2013 CE ranges from -100‰ to -70‰ within the NADW in the east (Figure 2b; Figure 3b), however, this large variability might also be due to a critical time when there is slight bomb ^{14}C incursion nearby as seen in the central Atlantic (see section 3.2). Again, this is not seen in the corals, as they integrate sub-decadal ^{14}C signals (Table S1).

The $\Delta^{14}C$ trend recorded in coral calcitic skeleton is similar to the central sites, both showing

low values prior to the 1960s and high values after the 1960s, except a single data point from Kni_1985m which shows early ^{14}C enrichment in the 1950s (Figure 3b). This may indicate an early signal to this deepest site, however, given the singular nature of this datapoint we will not over interpret this as an early onset at this particular site, but we cannot rule it out.

The comparison to seawater data in the east is more complex than in the central location given the wider range of data. Prior to 2013 CE, we generally observe coral $\Delta^{14}C$ similar to or higher than nearby seawater $\Delta^{14}C$ (Figure 3b). Modern oceanographic observations indicate interannual or even seasonal variability in the properties of AAIW (Fu et al., 2019; Roque et al., 2019), giving rise to the potential for relatively rapid changes in seawater $\Delta^{14}C$. Given that coral $\Delta^{14}C$ represents an averaged integrated signal over several years (Table S1), we would not expect to see all seawater fluctuations recorded in the coral.

3.2 Timescales of bomb ^{14}C transport

Seawater $\Delta^{14}C$ profiles around Vay_1455m, Vem_1474m, and Kni_1985m show the influence of bomb ^{14}C by 2013 CE (Figure 2a). However, as noted above, none of the corals in this study show bomb ^{14}C recorded in the calcitic skeleton (Figure 3). Although there are $\Delta^{14}C$ increases between 1960s and 1980s recorded in all four corals, we argue that the increases do not reflect the influence of bomb ^{14}C. The $\Delta^{14}C$ of the northern hemisphere atmosphere increased rapidly since the 1950s due to nuclear testing (Figure 4a; (Hua et al., 2013)). The ocean-atmosphere equilibration timescale is about 10 years depending on locations (Graven et al., 2012). Together with the transport time through the northern North Atlantic to the tropical Atlantic, the coral sites are unlikely to be influenced by the bomb ^{14}C as early as 1970s or 1980s. For instance, it took ~35 years for subtropical Atlantic intermediate water to respond to the atmosphere bomb ^{14}C pulse (Figure 4e; (Lee et al., 2017)). Therefore, it is unlikely for these more southern and deeper tropical intermediate waters to be influenced by bomb ^{14}C before 1990 CE.

Apart from the North Atlantic, the additional ^{14}C could potentially be bomb ^{14}C moving north from the South Atlantic since the observed seawater profiles show $\Delta^{14}C$ in mAAIW around Vay_1455m in 1983 CE increased compared to 1973 CE, suggesting potential bomb ^{14}C in mAAIW (Figure 2a). However, the ^{14}C of South Atlantic intermediate water is more depleted than North Atlantic, it is unlikely that bomb ^{14}C from South Atlantic leads the ^{14}C enrichment.

The discrepancy between coral records and seawater profiles suggests the bomb ^{14}C had only just arrived atVay_1455m site by the time coral Vay_1455m was collected, which is ~60 years later than the atmosphere (Figure 4), thus the temporal resolution of the coral subsampling is not high enough to distinguish the incorporation of this enriched bomb ^{14}C. The climate model, however, does imply that bomb ^{14}C penetration to Vay_1455m site occurred at around ~2000 CE (Figure 3a), some 10 years earlier than seawater and coral $\Delta^{14}C$ suggested. For the eastern Atlantic, there is no bomb signal observed in seawater nor coral $\Delta^{14}C$ around the Car_1409m site (Figure 3b), suggesting even later bomb penetration for the eastern Atlantic.

Coral $\Delta^{14}C$ records have previously been used to investigate the transport timescales of bomb ^{14}C to the northwest Atlantic (Figure 4) (Farmer et al., 2015b; Lee et al., 2017; Sherwood et al., 2008). For example, the marked increase of $\Delta^{14}C$ in 1983 CE at 700 m on the Grand Banks (44°N; Figure 1a, d; Sherwood et al., 2008) occurred ~27 years after the atmosphere, which is ~15 years later than model outputs (Figure 4c). The response times of coral $\Delta^{14}C$ records at 40°N (Figure 1a, d; Farmer et al., 2015b) and 32°N (Figure 1a, d; Lee et al., 2017) are both around 1990 CE, suggesting a decade later than model outputs (Figure 4d, e). The comparison between model outputs and coral records from our coral records and previous studies suggests a decade later arrival of bomb ^{14}C as indicated by coral records from North Atlantic than model outputs (Figure 4).

The decade-long delay of bomb ^{14}C transportation indicated by our combined coral and

seawater records compared to model outputs suggest modelled ^{14}C transport rates are too rapid. Previous studies have shown that the Deep Western Boundary Current (DWBC) is the fastest pathway for NADW transport from North Atlantic to South Atlantic (Rhein et al., 2015), although other ocean interior pathways exist, especially in the subpolar Atlantic and the transition between subpolar and subtropical gyre (Liu et al., 2024). For instance, the bomb ^{14}C transport timescale has been used to estimate the advection and mixing contribution ratio to ^{14}C transport, suggesting a comparable contribution of mixing and advection (Lee et al., 2017). For the tropical Atlantic, the DWBC has been suggested to be the main pathway for NADW. The transport of bomb ^{14}C to the coral location is mainly through the DWBC (Groeskamp et al., 2016), therefore, the bomb ^{14}C transport timescale could provide constraints on the DWBC transport rate. The late arrival of bomb ^{14}C to the deep ocean recorded by tropical Atlantic corals suggests a less efficient DWBC transport than climate models suggest, by around a decade (Figure 4f; Graven et al., 2012). Reconstructing the transport timescale of bomb ^{14}C using CWCs has the potential to provide additional constraints on the timescale of deep ocean circulation.

3.3 Bamboo coral calcitic $\Delta^{14}C$ reveals changes in water mass configuration over the last century

The three corals collected around 1500 m in the tropical Atlantic have the sensitivity to track the relative contribution of NADW and mAAIW due to the distinct $\Delta^{14}C$ values of the two water masses. Coral calcitic skeletons record constant $\Delta^{14}C$ between ~1830 CE and ~1960 CE (Figure 3), suggesting a relatively constant contribution of NADW and AAIW. However, there is an increase in coral $\Delta^{14}C$ between ~1960 CE and ~1980 CE across the central and eastern tropical Atlantic (Figure 3). Several possibilities may have caused this increase in seawater $\Delta^{14}C$: (1) uncertainty in the age models causing calculated $\Delta^{14}C$ to be incorrect; (2) the

influence of metabolic carbon derived from the surface ocean; (3) enhanced seawater ventilation; (4) the source natural ^{14}C from atmosphere enriched; (5) bomb ^{14}C penetration; (6) a change in water-mass configuration. Below, we argue that the sixth scenario is most plausible.

Because it is age-corrected, the $\Delta^{14}C$ of each subsample is influenced by the time when the skeleton was formed (Equation 2). An incorrect age model would lead to errors in the calculated $\Delta^{14}C$. In this study, the age model of each coral is independent from each other and independent from ^{14}C (section 2.4) so that it is unlikely that the age of all three corals would cause the systematic shifts in $\Delta^{14}C$ during the same time period.

Inclusion of metabolic carbon from surface waters also has the potential to influence bamboo coral calcitic $\Delta^{14}C$. Indeed, a previous study suggests that up to 8% carbon could be derived from metabolic carbon in the skeleton of scleractinian corals collected from the tropical intermediate Pacific (Adkins et al., 2003). We have already shown that the $\Delta^{14}C$ of the organic node of bamboo corals (reflecting near surface water) increased from the ~1960 CE due to the incorporation of bomb ^{14}C (Figure 4f; (Liu et al., 2023; Roark et al., 2005)). Based on the $\Delta^{14}C$ of the corresponding organic node (Liu et al., 2023), an increase of 5 to 9% metabolic carbon would be needed to cause the shift in the calcite $\Delta^{14}C$ enrichment observed. Such levels of metabolic carbon incorporation into calcitic skeletons are perhaps not unreasonable when compared to the 8% metabolic carbon in scleractinian coral skeletons (Adkins et al., 2003), however, there are two factors which suggest that this mechanism is not likely to be the cause of the shift. Firstly, in the scenario that the incorporation of metabolic carbon into calcitic skeleton of bamboo corals occurs continuously during the coral lifespan and in all the bamboo corals, a further increase in the calcitic $\Delta^{14}C$ after 1980s would be expected because the peak $\Delta^{14}C$ in the organic nodes occurred in 1990s (Figure 4f). This late increase is, however, not observed in the calcitic skeleton of this study (Figure 4g). In addition, there is no such

enrichment observed in the calcitic skeleton of a northwest Atlantic (Grand Banks) bamboo coral (Figure 4c) where the food source was also influenced by bomb ^{14}C indicated by the increased $\Delta^{14}C$ in organic node (Sherwood et al., 2008), suggesting the metabolic carbon is not a significant source to the bamboo coral calcitic skeleton. Secondly, even if metabolic carbon influences were significant, it is extremely unlikely that all four corals were influenced by a shift in the amount of incorporated metabolic carbon at the same time across the central and eastern Atlantic. Therefore, metabolic carbon is unlikely to be the main contributor to the enrichment of $\Delta^{14}C$ in the calcitic skeleton between 1960s and 1980s.

After excluding age model and metabolic carbon influences, the shift in $\Delta^{14}C$ is most likely to reflect an increase in seawater $\Delta^{14}C$ between 1960s and 1980s. This could be the results of enhanced ventilation or the introduction of an additional ^{14}C source. Enhanced ventilation would lead to less ^{14}C decayed after leaving surface ocean. However, ventilation related ^{14}C changes would operate on a longer timescale (e.g., centennial variation) than the two decades in question here. This is due to the ~ 60 years transportation time required for changes in water masses to reach the coral sites, as discussed in Section 3.2. Moreover, even a doubling of AMOC strength would only reduce transport time by ~30 years, resulting in a lead to a $\Delta^{14}C$ increase of approximately 3 ‰ – far less than the observed 9‰ increase. Therefore, we do not consider enhanced ventilation is responsible to the $\Delta^{14}C$ increase.

Additional ^{14}C sources could potentially be either an enrichment of natural ^{14}C in atmosphere, bomb ^{14}C, or natural water mass mixing. We rule out bomb ^{14}C in the first place as discussed in Section 3.2 that bomb ^{14}C is unlikely to invade the coral locations before 1990 CE. In addition, we can rule out enrichment of natural ^{14}C as no ^{14}C enrichment before bomb ^{14}C in the atmosphere was observed (Figure 4a). Therefore, both natural ^{14}C from atmosphere and bomb ^{14}C can be excluded as an additional ^{14}C source.

406 Instead of an atmospheric ^{14}C source, a more plausible explanation for this shift in coral $\Delta^{14}C$
407 is a change in water-mass configuration. The relative contribution of ^{14}C enriched NADW and
408 ^{14}C depleted mAAIW is one of the key factors that influences seawater $\Delta^{14}C$ at these sites. The
409 enriched ^{14}C in the coral locations is therefore the result of more (less) influence of NADW
410 (mAAIW) from the 1960s to 1980s. Two mechanisms potentially explain the increase in
411 NADW contribution at the expense of mAAIW at our coral sites (Figure 5): (1) the depth range
412 of NADW became shallower or thicker during this period; and/or (2) the NACW and SACW
413 shifted southward and deepened with mAAIW retreating in response to slowdown of AMOC.
414 Here we examine some of the wider oceanographic changes that may have influenced the coral
415 sites.

416 Multiple proxies have suggested a weakened AMOC during the 1970s (Figure 6), including
417 northern North Atlantic surface temperature anomaly as constrained by both model simulations
418 and direct observations (Caesar et al., 2018; Pontes and Menviel, 2024; Rahmstorf et al., 2015).
419 Western North Atlantic benthic foraminifera $\delta^{18}O$ records show subsurface warming between
420 the 1960s and 1980s, which is interpreted as an accumulation of heat in the subsurface due to
421 weakened AMOC (Thibodeau et al., 2018). Similarly, western North Atlantic $\delta^{15}N$ recorded in
422 deep-sea gorgonian coral *Primnoa resedaeformis* over the Canadian shelf decreased between
423 the 1960s and 1980s (Figure 6d), suggesting an increase in the proportion of Atlantic warm
424 slope water linked to weakened AMOC (Sherwood et al., 2011). During the same period, Arctic
425 sea ice extent decreased rapidly (Figure 6e), indicating increased fluxes of fresh water to the
426 North Atlantic (Kinnard et al., 2011). The historical simulations in CMIP6 models also indicate
427 an abrupt decline of AMOC in the 1980s (Weijer et al., 2020) or since the 1950s when
428 freshwater forcing is incorporated (Pontes and Menviel, 2024).

429 One of the pronounced features of this declining AMOC is the weakened formation of Labrador

Slope Water (LSW) due to increased input of fresh water (Caesar et al., 2018; Pontes and Menviel, 2024; Thibodeau et al., 2018; Thornalley et al., 2018), which would result in a lower density LSW and potentially a shallower NADW. The shallower NADW further immerses the coral locations with higher ^{14}C content. In this scenario, the calcitic $\Delta^{14}C$ recorded in the four corals across the tropical Atlantic would increase along with the weakened AMOC. The timings of the ^{14}C-enrichment recorded in the calcitic skeleton agree with the AMOC proxies despite subtle leads and lags that can be attributed to either the different resolution and/or time integration of the respective proxies.

The $\Delta^{14}C$ recorded in the corals collected from Grand Banks (44°N; Figure 4c), Georges Banks (40°N; Figure 4d) and Bermuda (32°N; Figure 4e) do not show the same shift observed in our study sites. This is not unexpected, as these locations are too far north to be directly influenced by mAAIW and their respective water column profiles do not have strong $\Delta^{14}C$ gradients (Figure 1a; Figure 5) (Talley, 1996).

Additional changes to water masses configuration might also involve the southward shift of NACW and SACW in the subtropical/tropical North Atlantic, leading to the retreat of mAAIW in response to the slowdown of AMOC. Benthic foraminiferal Mg/Ca temperature reconstructions of Atlantic waters during the last deglaciation suggest a potential southward shift of NACW and SACW and a deepened thermocline during intervals of AMOC slowdown (Huang et al., 2012; Stewart et al., 2023). With a southward and deepened NACW and SACW, mAAIW might retreat southward (Gu et al., 2017; Morley et al., 2011). Indeed, model simulation results suggested a deepened thermocline in the tropical Atlantic after the 1980s (Lozier et al., 2010). In addition, previous studies have indicated that the production and northward extent of AAIW weakened over the last 50 years (Curry et al., 2003; Goes et al., 2008). If this water mass shifted southward, the coral locations would be more influenced by

454 the ^{14}C-enriched water mass (Figure 3), thus explaining the $\Delta^{14}C$ enrichment between the 1960s
455 and 1980s. Our findings suggest that the seawater $\Delta^{14}C$ recorded in tropical CWCs exhibits a
456 clear link to AMOC strength. In this regard, ^{14}C or nutrient records from the northern front of
457 mAAIW covering the last century would also be of value.

458 The synchronization between the rise in $\Delta^{14}C$ from the 1960s to the 1980s, observed in our
459 coral records, and the high latitude North Atlantic AMOC indices suggests that the oceanic
460 reconfiguration was a synchronous process rather than a signal transported from the high
461 latitude North Atlantic. This reconfiguration occurred not only in the subpolar regions but also
462 in the tropical regions, affecting both surface and intermediate waters. Additionally, the $\Delta^{14}C$
463 increase during this period corresponds to tropical North Atlantic surface variations. Decline
464 in tropical North Atlantic upwelling since the 1970s, revealed through box model calculations
465 using sea surface $\Delta^{14}C$ records (Figure 6f; (Paterne et al., 2023)), align with reduced advection
466 of Sub-Antarctic Mode Water (Toggweiler et al., 2019a, 2019b). Concurrently, decreased sea
467 surface salinity in the western tropical South Atlantic, indicated by shallow water coral $\delta^{18}O$
468 records (Figure 6h; (Pereira et al., 2022)), corresponds with a diminished interhemispheric
469 Atlantic sea-surface temperature gradient (Figure 6g; (Kennedy et al., 2019)), leading to a
470 southward migration of the intertropical convergence zone (Thompson et al., 2010).

471 The coherence between high latitude AMOC indices, tropical Atlantic surface variations, and
472 intermediate water mass changes highlights a significant large-scale reconfiguration of oceanic
473 circulation during the 1960s and 1980s.

474

4. Conclusions

The $\Delta^{14}C$ of tropical Atlantic intermediate seawater since the Industrial Revolution is reconstructed from the calcitic skeleton of four cold-water bamboo corals. The records were dated independently using band-counting derived growth rates in the corresponding organic nodes. No bomb ^{14}C was recorded in the coral calcitic skeleton, suggesting that the tropical Atlantic had not been invaded by bomb radiocarbon at the time of coral collection or had only just arrived (as indicated by seawater $\Delta^{14}C$ profiles), suggesting a ~60 years transportation timescale. This study thus provides valuable sub-decadal records for ocean transport models to further constrain deep ocean circulation on decadal timescales. Seawater $\Delta^{14}C$ in tropical Atlantic intermediate water was relatively constant between 1830 CE to 1960 CE and then increased between the 1960s and 1980s at both central and eastern sites. The increase of seawater $\Delta^{14}C$ is potentially related to weakened AMOC, which may lead to a shallower NADW and/or a southward retreat of AAIW, both likely accounting for the enriched ^{14}C signal between the 1960s and 1980s. Our study thus provides the first coral ^{14}C dataset from tropical Atlantic intermediate waters for the last century that addresses the potential changes in water mass configuration in response to a weakening of AMOC. Our records suggest that the water mass reconfiguration in tropical Atlantic intermediate water is not a local phenomenon, but a large-scale reconfiguration of oceanic circulation. Such reconfiguration will make significant impact on the heat and carbon uptake and redistribution of the ocean, which will further influence the climate.

Acknowledgements

We acknowledge the crew and researchers on board the research cruise JC094 (Equatorial Atlantic in 2013) who obtained the samples for this study. We thank Oliver Andrews for his

support on Earth System Model data extraction and analysis. We thank Christopher Coath, Carolyn Taylor for their help with laboratory work. Funding was provided by National Key Research and Development Program of China (2023YFF0806100), China Postdoctoral Science Foundation (2024M763370), China Scholarship Council to Q.L., ERC and NERC grants awarded to L.F.R. (278705, NE/S001743/1 and NE/R005117/1).

APPENDIX A. Supplementary Material

The following are the Supplementary material to this article: Supplementary text, including Figure A1. Supplementary data: Research data, including Table S1, Table S2.

References

Adkins, J.F., Boyle, E.A., Curry, W.B., Lutringer, A., 2003. Stable isotopes in deep-sea corals and a new mechanism for "vital effects." Geochimica et Cosmochimica Acta 67, 1129–1143. https://doi.org/10.1016/S0016-7037(02)01203-6

Adkins, J.F., Cheng, H., Boyle, E.A., Druffel, E.R.M., Edwards, R.L., 1998. Deep-Sea Coral Evidence for Rapid Change in Ventilation of the Deep North Atlantic 15,400 Years Ago. Science 280, 725–728. https://doi.org/10.1126/science.280.5364.725

Adkins, J.F., Griffin, S., Kashgarian, M., Cheng, H., Druffel, E.R.M., Boyle, E.A., Edwards, R.L., Shen, C.-C., 2002. Radiocarbon Dating of Deep-Sea Corals. Radiocarbon 44, 567–580. https://doi.org/10.1017/S0033822200031921

Azetsu-Scott, K., Jones, E.P., Gershey, R.M., 2005. Distribution and ventilation of water masses in the Labrador Sea inferred from CFCs and carbon tetrachloride. Marine Chemistry, Analytical and Marine Chemistry: A Tribute to Professor David Dyrssen, the founding father of Swedish Marine Chemistry 94, 55–66. https://doi.org/10.1016/j.marchem.2004.07.015

Broecker, W.S., 1991. The Great Ocean Conveyor. oceanog 4, 79–89. https://doi.org/10.5670/oceanog.1991.07

Broecker, W.S., Gerard, R., Ewing, M., Heezen, B.C., 1960. Natural radiocarbon in the Atlantic Ocean. Journal of Geophysical Research (1896-1977) 65, 2903–2931. https://doi.org/10.1029/JZ065i009p02903

Broecker, W.S., Peng, T.-H., Stuiver, M., 1978. An estimate of the upwelling rate in the equatorial Atlantic based on the distribution of bomb radiocarbon. Journal of Geophysical Research: Oceans 83, 6179–6186. https://doi.org/10.1029/JC083iC12p06179

Bub, F.L., Brown, W.S., 1996. Intermediate layer water masses in the western tropical Atlantic Ocean. Journal of Geophysical Research: Oceans 101, 11903–11922. https://doi.org/10.1029/95JC03372

Burke, A., Robinson, L.F., 2012. The Southern Ocean's Role in Carbon Exchange During the Last Deglaciation. Science 335, 557–561. https://doi.org/10.1126/science.1208163

Caesar, L., McCarthy, G.D., Thornalley, D.J.R., Cahill, N., Rahmstorf, S., 2021. Current Atlantic Meridional Overturning Circulation weakest in last millennium. Nat. Geosci. 14, 118–120. https://doi.org/10.1038/s41561-021-00699-z

Caesar, L., Rahmstorf, S., Robinson, A., Feulner, G., Saba, V., 2018. Observed fingerprint of a weakening Atlantic Ocean overturning circulation. Nature 556, 191–196. https://doi.org/10.1038/s41586-018-0006-5

Chen, T., Robinson, L.F., Burke, A., Southon, J., Spooner, P., Morris, P.J., Ng, H.C., 2015. Synchronous centennial abrupt events in the ocean and atmosphere during the last deglaciation. Science 349, 1537–1541. https://doi.org/10.1126/science.aac6159

Curry, R., Dickson, B., Yashayaev, I., 2003. A change in the freshwater balance of the Atlantic Ocean over the past four decades. Nature 426, 826–829. https://doi.org/10.1038/nature02206

Danabasoglu, G., 2019. NCAR CESM2 model output prepared for CMIP6 CMIP historical. https://doi.org/10.22033/ESGF/CMIP6.7627

Druffel, E., 2002. Radiocarbon in Corals: Records of the Carbon Cycle, Surface Circulation and Climate. oceanog 15, 122–127. https://doi.org/10.5670/oceanog.2002.43

Druffel, E.M., 1980. Radiocarbon in Annual Coral Rings of Belize and Florida. Radiocarbon 22, 363–371. https://doi.org/10.1017/S0033822200009656

Emery, W., Meincke, J., 1986. Global water masses - summary and review. Oceanologica Acta 9, 383–391.

Farmer, J.R., Hönisch, B., Robinson, L.F., Hill, T.M., 2015a. Effects of seawater-pH and biomineralization on the boron isotopic composition of deep-sea bamboo corals. Geochimica et Cosmochimica Acta 155, 86–106. https://doi.org/10.1016/j.gca.2015.01.018

Farmer, J.R., Robinson, L.F., Hönisch, B., 2015b. Growth rate determinations from radiocarbon in bamboo corals (genus *Keratoisis*). Deep Sea Research Part I: Oceanographic Research Papers 105, 26–40. https://doi.org/10.1016/j.dsr.2015.08.004

Fernandez, A., Lapen, T.J., Andreasen, R., Swart, P.K., White, C.D., Rosenheim, B.E., 2015. Ventilation time scales of the North Atlantic subtropical cell revealed by coral radiocarbon from the Cape Verde Islands. Paleoceanography 30, 938–948. https://doi.org/10.1002/2015PA002790

Fu, Y., Karstensen, J., Brandt, P., 2018. Atlantic Meridional Overturning Circulation at 14.5° N in 1989 and 2013 and 24.5° N in 1992 and 2015: volume, heat, and freshwater transports. Ocean Science 14, 589–616. https://doi.org/10.5194/os-14-589-2018

Geyman, B.M., Ptacek, J.L., LaVigne, M., Horner, T.J., 2019. Barium in deep-sea bamboo corals: Phase associations, barium stable isotopes, & prospects for paleoceanography. Earth and Planetary Science Letters 525, 115751. https://doi.org/10.1016/j.epsl.2019.115751

Godwin, H., 1962. Radiocarbon Dating: Fifth International Conference. Nature 195, 943–945. https://doi.org/10.1038/195943a0

Goes, M., Wainer, I., Gent, P.R., Bryan, F.O., 2008. Changes in subduction in the South Atlantic Ocean during the 21st century in the CCSM3. Geophysical Research Letters 35. https://doi.org/10.1029/2007GL032762

Grammer, G.L., Fallon, S.J., Izzo, C., Wood, R., Gillanders, B.M., 2015. Investigating bomb radiocarbon transport in the southern Pacific Ocean with otolith radiocarbon. Earth and Planetary Science Letters 424, 59–68. https://doi.org/10.1016/j.epsl.2015.05.008

Graven, H.D., 2015. Impact of fossil fuel emissions on atmospheric radiocarbon and various applications of radiocarbon over this century. Proceedings of the National Academy of Sciences 112, 9542–9545. https://doi.org/10.1073/pnas.1504467112

Graven, H.D., Gruber, N., Key, R., Khatiwala, S., Giraud, X., 2012. Changing controls on oceanic radiocarbon: New insights on shallow-to-deep ocean exchange and anthropogenic CO2 uptake. Journal of Geophysical Research: Oceans 117. https://doi.org/10.1029/2012JC008074

Groeskamp, S., Lenton, A., Matear, R., Sloyan, B.M., Langlais, C., 2016. Anthropogenic carbon in the ocean—Surface to interior connections. Global Biogeochemical Cycles 30, 1682–1698. https://doi.org/10.1002/2016GB005476

Gu, S., Liu, Z., Zhang, J., Rempfer, J., Joos, F., Oppo, D.W., 2017. Coherent Response of Antarctic Intermediate Water and Atlantic Meridional Overturning Circulation During the Last Deglaciation: Reconciling Contrasting Neodymium Isotope Reconstructions From the Tropical Atlantic. Paleoceanography 32, 1036–1053. https://doi.org/10.1002/2017PA003092

Hu, A., Roekel, L.V., Weijer, W., Garuba, O.A., Cheng, W., Nadiga, B.T., 2020. Role of AMOC in Transient Climate Response to Greenhouse Gas Forcing in Two Coupled Models. Journal of Climate. https://doi.org/10.1175/JCLI-D-19-1027.1

Hua, Q., Barbetti, M., Rakowski, A.Z., 2013. Atmospheric Radiocarbon for the Period 1950–2010. Radiocarbon 55, 2059–2072. https://doi.org/10.2458/azu_js_rc.v55i2.16177

Huang, E., Mulitza, S., Paul, A., Groeneveld, J., Steinke, S., Schulz, M., 2012. Response of eastern tropical Atlantic central waters to Atlantic meridional overturning circulation changes during the Last Glacial Maximum and Heinrich Stadial 1. Paleoceanography 27. https://doi.org/10.1029/2012PA002294

Huang, K.-F., Oppo, D.W., Curry, W.B., 2014. Decreased influence of Antarctic intermediate water in the tropical Atlantic during North Atlantic cold events. Earth and Planetary Science Letters 389, 200–208. https://doi.org/10.1016/j.epsl.2013.12.037

Jenkins, W.J., Smethie, W.M., Boyle, E.A., Cutter, G.A., 2015. Water mass analysis for the U.S. GEOTRACES (GA03) North Atlantic sections. Deep Sea Research Part II: Topical Studies in Oceanography, GEOTRACES GA-03 - The U.S. GEOTRACES North Atlantic Transect 116, 6–20. https://doi.org/10.1016/j.dsr2.2014.11.018

Kennedy, J.J., Rayner, N.A., Atkinson, C.P., Killick, R.E., 2019. An Ensemble Data Set of Sea Surface Temperature Change From 1850: The Met Office Hadley Centre HadSST.4.0.0.0 Data Set. Journal of Geophysical Research: Atmospheres 124, 7719–7763. https://doi.org/10.1029/2018JD029867

Kilbourne, K.H., Wanamaker, A.D., Moffa-Sanchez, P., Reynolds, D.J., Amrhein, D.E., Butler, P.G., Gebbie, G., Goes, M., Jansen, M.F., Little, C.M., Mette, M., Moreno-Chamarro, E., Ortega, P., Otto-Bliesner, B.L., Rossby, T., Scourse, J., Whitney, N.M., 2022. Atlantic circulation change still uncertain. Nat. Geosci. 15, 165–167. https://doi.org/10.1038/s41561-022-00896-4

Kinnard, C., Zdanowicz, C.M., Fisher, D.A., Isaksson, E., de Vernal, A., Thompson, L.G., 2011. Reconstructed changes in Arctic sea ice over the past 1,450 years. Nature 479, 509–512. https://doi.org/10.1038/nature10581

Kirchner, K., Rhein, M., Hüttl-Kabus, S., Böning, C.W., 2009. On the spreading of South Atlantic Water into the Northern Hemisphere. Journal of Geophysical Research: Oceans 114. https://doi.org/10.1029/2008JC005165

Knowles, T.D.J., Monaghan, P.S., Evershed, R.P., 2019. Radiocarbon Sample Preparation Procedures and the First Status Report from the Bristol Radiocarbon AMS (BRAMS) Facility. Radiocarbon 61, 1541–1550. https://doi.org/10.1017/RDC.2019.28

Kromer, R.W. a. B., 2014. Temperature, salinity and other variables collected from discrete sample and profile observations using CTD, bottle and other instruments from the METEOR in the North Atlantic Ocean and South Atlantic Ocean from 1981-03-28 to 1981-04-23 (NODC Accession 0116646). Version 1.1. NationalOceanographic Data Center, NOAA. Dataset.

LaVigne, M., Hill, T.M., Spero, H.J., Guilderson, T.P., 2011. Bamboo coral Ba/Ca: Calibration of a new deep ocean refractory nutrient proxy. Earth and Planetary Science Letters 312, 506–515. https://doi.org/10.1016/j.epsl.2011.10.013

Lee, J.-M., Eltgroth, S.F., Boyle, E.A., Adkins, J.F., 2017. The transfer of bomb radiocarbon and anthropogenic lead to the deep North Atlantic Ocean observed from a deep sea coral. Earth and Planetary Science Letters 458, 223–232. https://doi.org/10.1016/j.epsl.2016.10.049

Liu, Q., Robinson, L.F., Hendy, E., Prokopenko, M.G., Stewart, J.A., Knowles, T.D.J., Li, T., Samperiz, A., 2023. Reinterpreting radiocarbon records in bamboo corals – New insights from the tropical North Atlantic. Geochimica et Cosmochimica Acta 348, 296–308. https://doi.org/10.1016/j.gca.2023.03.019

Liu, W., Fedorov, A.V., Xie, S.-P., Hu, S., 2020. Climate impacts of a weakened Atlantic Meridional Overturning Circulation in a warming climate. Science Advances 6, eaaz4876. https://doi.org/10.1126/sciadv.aaz4876

Liu, Z., Gu, S., Zou, S., Zhang, S., Yu, Y., He, C., 2024. Wind-steered Eastern Pathway of the Atlantic Meridional Overturning Circulation. Nat. Geosci. 17, 353–360. https://doi.org/10.1038/s41561-024-01407-3

Lower-Spies, E.E., Whitney, N.M., Wanamaker, A.D., Griffin, S.M., Introne, D.S., Kreutz, K.J., 2020. A 250-Year, Decadally Resolved, Radiocarbon Time History in the Gulf of Maine Reveals a Hydrographic Regime Shift at the End of the Little Ice Age. Journal of Geophysical Research: Oceans 125, e2020JC016579. https://doi.org/10.1029/2020JC016579

Lozier, M.S., Roussenov, V., Reed, M.S.C., Williams, R.G., 2010. Opposing decadal changes for the North Atlantic meridional overturning circulation. Nature Geosci 3, 728–734. https://doi.org/10.1038/ngeo947

Lynch-Stieglitz, J., Vollmer, T.D., Valley, S.G., Blackmon, E., Gu, S., Marchitto, T.M., 2024. A diminished North Atlantic nutrient stream during Younger Dryas climate reversal. Science 384, 693–696. https://doi.org/10.1126/science.adi5543

Morley, A., Schulz, M., Rosenthal, Y., Mulitza, S., Paul, A., Rühlemann, C., 2011. Solar modulation of North Atlantic central Water formation at multidecadal timescales during the late Holocene. Earth and Planetary Science Letters 308, 161–171. https://doi.org/10.1016/j.epsl.2011.05.043

Noé, S.U., Dullo, W.-Chr., 2006. Skeletal morphogenesis and growth mode of modern and fossil deep-water isidid gorgonians (Octocorallia) in the West Pacific (New Zealand and Sea of Okhotsk). Coral Reefs 25, 303–320. https://doi.org/10.1007/s00338-006-0095-8

Olsen, A., Lange, N., Key, R.M., Tanhua, T., Álvarez, M., Becker, S., Bittig, H.C., Carter, B.R., Cotrim da Cunha, L., Feely, R.A., van Heuven, S., Hoppema, M., Ishii, M., Jeansson, E., Jones, S.D., Jutterström, S., Karlsen, M.K., Kozyr, A., Lauvset, S.K., Lo Monaco, C., Murata, A., Pérez, F.F., Pfeil, B., Schirnick, C., Steinfeldt, R., Suzuki, T., Telszewski, M., Tilbrook, B., Velo, A., Wanninkhof, R., 2019. GLODAPv2.2019 – an update of GLODAPv2. Earth System Science Data 11, 1437–1461. https://doi.org/10.5194/essd-11-1437-2019

Olsen, A., Lange, N., Key, R.M., Tanhua, T., Bittig, H.C., Kozyr, A., Álvarez, M., Azetsu-Scott, K., Becker, S., Brown, P.J., Carter, B.R., Cotrim da Cunha, L., Feely, R.A., van Heuven, S., Hoppema, M., Ishii, M., Jeansson, E., Jutterström, S., Landa, C.S., Lauvset, S.K., Michaelis, P., Murata, A., Pérez, F.F., Pfeil, B., Schirnick, C., Steinfeldt, R., Suzuki, T., Tilbrook, B., Velo, A., Wanninkhof, R., Woosley, R.J., 2020. An updated version of the global interior ocean biogeochemical data product, GLODAPv2.2020. Earth System Science Data 12, 3653–3678. https://doi.org/10.5194/essd-12-3653-2020

Orr, J.C., Najjar, R.G., Aumont, O., Bopp, L., Bullister, J.L., Danabasoglu, G., Doney, S.C., Dunne, J.P., Dutay, J.-C., Graven, H., Griffies, S.M., John, J.G., Joos, F., Levin, I., Lindsay, K., Matear, R.J., McKinley, G.A., Mouchet, A., Oschlies, A., Romanou, A., Schlitzer, R., Tagliabue, A., Tanhua, T., Yool, A., 2017. Biogeochemical protocols and diagnostics for the CMIP6 Ocean Model Intercomparison Project (OMIP). Geoscientific Model Development 10, 2169–2199. https://doi.org/10.5194/gmd-10-2169-2017

Pahnke, K., Goldstein, S.L., Hemming, S.R., 2008. Abrupt changes in Antarctic Intermediate Water circulation over the past 25,000 years. Nature Geosci 1, 870–874. https://doi.org/10.1038/ngeo360

Paterne, M., Druffel, E.R.M., Guilderson, T.P., Blamart, D., Moreau, C., Weil-Accardo, J., Feuillet, N., 2023. Pulses of South Atlantic water into the tropical North Atlantic since 1825 from coral isotopes. Science Advances 9, eadi1687. https://doi.org/10.1126/sciadv.adi1687

Pedro, J.B., Jochum, M., Buizert, C., He, F., Barker, S., Rasmussen, S.O., 2018. Beyond the bipolar seesaw: Toward a process understanding of interhemispheric coupling. Quaternary Science Reviews 192, 27–46. https://doi.org/10.1016/j.quascirev.2018.05.005

Pereira, N.S., Clarke, L.J., Chiessi, C.M., Kilbourne, K.H., Crivellari, S., Cruz, F.W., Campos, J.L.P.S., Yu, T.-L., Shen, C.-C., Kikuchi, R.K.P., Pinheiro, B.R., Longo, G.O., Sial, A.N., Felis, T., 2022. Mid to late 20th century freshening of the western tropical South Atlantic triggered by southward migration of the Intertropical Convergence Zone. Palaeogeography, Palaeoclimatology, Palaeoecology 597, 111013. https://doi.org/10.1016/j.palaeo.2022.111013

Pontes, G.M., Menviel, L., 2024. Weakening of the Atlantic Meridional Overturning Circulation driven by subarctic freshening since the mid-twentieth century. Nat. Geosci. 1–8. https://doi.org/10.1038/s41561-024-01568-1

Poole, R., Tomczak, M., 1999. Optimum multiparameter analysis of the water mass structure in the Atlantic Ocean thermocline. Deep Sea Research Part I: Oceanographic Research Papers 46, 1895–1921. https://doi.org/10.1016/S0967-0637(99)00025-4

Rafter, P.A., Gray, W.R., Hines, S.K.V., Burke, A., Costa, K.M., Gottschalk, J., Hain, M.P., Rae, J.W.B., Southon, J.R., Walczak, M.H., Yu, J., Adkins, J.F., DeVries, T., 2022. Global reorganization of deep-sea circulation and carbon storage after the last ice age. Science Advances 8, eabq5434. https://doi.org/10.1126/sciadv.abq5434

Rahmstorf, S., 2024. FEATURE ARTICLE Is the Atlantic Overturning Circulation Approaching a Tipping Point? Oceanography 37, 16–29. https://doi.org/10.5670/oceanog.2024.501

Rahmstorf, S., Box, J.E., Feulner, G., Mann, M.E., Robinson, A., Rutherford, S., Schaffernicht, E.J., 2015. Exceptional twentieth-century slowdown in Atlantic Ocean overturning circulation. Nature Clim Change 5, 475–480. https://doi.org/10.1038/nclimate2554

Rhein, M., Kieke, D., Steinfeldt, R., 2015. Advection of North Atlantic Deep Water from the Labrador Sea to the southern hemisphere. Journal of Geophysical Research: Oceans 120, 2471–2487. https://doi.org/10.1002/2014JC010605

Roark, E.B., Guilderson, T.P., Flood-Page, S., Dunbar, R.B., Ingram, B.L., Fallon, S.J., McCulloch, M., 2005. Radiocarbon-based ages and growth rates of bamboo corals from the Gulf of Alaska. Geophysical Research Letters 32. https://doi.org/10.1029/2004GL021919

Robinson, L.F., 2014. RRS James Cook Cruise JC094, October 13 – November 30 2013 Tenerife - Trinidad (Cruise report). https://epic.awi.de/id/eprint/35605/

Schmittner, A., 2005. Decline of the marine ecosystem caused by a reduction in the Atlantic overturning circulation. Nature 434, 628–633. https://doi.org/10.1038/nature03476

Serrato Marks, G., LaVigne, M., Hill, T.M., Sauthoff, W., Guilderson, T.P., Roark, E.B., Dunbar, R.B., Horner, T.J., 2017. Reproducibility of Ba/Ca variations recorded by northeast Pacific bamboo corals. Paleoceanography 32, 966–979. https://doi.org/10.1002/2017PA003178

Sherwood, O.A., Edinger, E.N., 2009. Ages and growth rates of some deep-sea gorgonian and antipatharian corals of Newfoundland and Labrador. Can. J. Fish. Aquat. Sci. 66, 142–152. https://doi.org/10.1139/F08-195

Sherwood, O.A., Edinger, E.N., Guilderson, T.P., Ghaleb, B., Risk, M.J., Scott, D.B., 2008. Late Holocene radiocarbon variability in Northwest Atlantic slope waters. Earth and Planetary Science Letters 275, 146–153. https://doi.org/10.1016/j.epsl.2008.08.019

Sherwood, O.A., Lehmann, M.F., Schubert, C.J., Scott, D.B., McCarthy, M.D., 2011. Nutrient regime shift in the western North Atlantic indicated by compound-specific δ^{15}N of deep-sea gorgonian corals. Proc. Natl. Acad. Sci. U.S.A. 108, 1011–1015. https://doi.org/10.1073/pnas.1004904108

Skinner, L.C., Bard, E., 2022. Radiocarbon as a Dating Tool and Tracer in Paleoceanography. Reviews of Geophysics 60, e2020RG000720. https://doi.org/10.1029/2020RG000720

Stewart, J.A., Robinson, L.F., Rae, J.W.B., Burke, A., Chen, T., Li, T., de Carvalho Ferreira, M.L., Fornari, D.J., 2023. Arctic and Antarctic forcing of ocean interior warming during the last deglaciation. Sci Rep 13, 22410. https://doi.org/10.1038/s41598-023-49435-0

Stramma, L., Schott, F., 1999. The mean flow field of the tropical Atlantic Ocean. Deep Sea Research Part II: Topical Studies in Oceanography 46, 279–303. https://doi.org/10.1016/S0967-0645(98)00109-X

Stuiver, M., Polach, H.A., 1977. Discussion Reporting of 14C Data. Radiocarbon 19, 355–363. https://doi.org/10.1017/S0033822200003672

Talley, L.D., 1996. Antarctic Intermediate Water in the South Atlantic, in: Wefer, G., Berger, W.H., Siedler, G., Webb, D.J. (Eds.), The South Atlantic: Present and Past Circulation. Springer, Berlin, Heidelberg, pp. 219–238. https://doi.org/10.1007/978-3-642-80353-6_11

Talley, L.D., Pickard, G.L., Emery, W.J., Swift, J.H., 2011. Chapter 9 - Atlantic Ocean, in: Talley, L.D., Pickard, G.L., Emery, W.J., Swift, J.H. (Eds.), Descriptive Physical Oceanography (Sixth Edition). Academic Press, Boston, pp. 245–301. https://doi.org/10.1016/B978-0-7506-4552-2.10009-5

Thibodeau, B., Not, C., Zhu, J., Schmittner, A., Noone, D., Tabor, C., Zhang, J., Liu, Z., 2018. Last Century Warming Over the Canadian Atlantic Shelves Linked to Weak Atlantic Meridional Overturning Circulation. Geophysical Research Letters 45, 12,376-12,385. https://doi.org/10.1029/2018GL080083

Thompson, D.W.J., Wallace, J.M., Kennedy, J.J., Jones, P.D., 2010. An abrupt drop in Northern Hemisphere sea surface temperature around 1970. Nature 467, 444–447. https://doi.org/10.1038/nature09394

Thornalley, D.J.R., Oppo, D.W., Ortega, P., Robson, J.I., Brierley, C.M., Davis, R., Hall, I.R., Moffa-Sanchez, P., Rose, N.L., Spooner, P.T., Yashayaev, I., Keigwin, L.D., 2018. Anomalously weak Labrador Sea convection and Atlantic overturning during the past 150 years. Nature 556, 227–230. https://doi.org/10.1038/s41586-018-0007-4

Timmermann, A., An, S.-I., Krebs, U., Goosse, H., 2005. ENSO Suppression due to Weakening of the North Atlantic Thermohaline Circulation. Journal of Climate 18, 3122–3139. https://doi.org/10.1175/JCLI3495.1

Toggweiler, J.R., Druffel, E.R.M., Key, R.M., Galbraith, E.D., 2019a. Upwelling in the Ocean Basins North of the ACC: 1. On the Upwelling Exposed by the Surface Distribution of Δ14C. Journal of Geophysical Research: Oceans 124, 2591–2608. https://doi.org/10.1029/2018JC014794

Toggweiler, J.R., Druffel, E.R.M., Key, R.M., Galbraith, E.D., 2019b. Upwelling in the Ocean Basins North of the ACC: 2. How Cool Subantarctic Water Reaches the Surface in the Tropics. Journal of Geophysical Research: Oceans 124, 2609–2625. https://doi.org/10.1029/2018JC014795

van Westen, R.M., Kliphuis, M., Dijkstra, H.A., 2024. Physics-based early warning signal shows that AMOC is on tipping course. Science Advances 10, eadk1189. https://doi.org/10.1126/sciadv.adk1189

Weijer, W., Cheng, W., Garuba, O.A., Hu, A., Nadiga, B.T., 2020. CMIP6 Models Predict Significant 21st Century Decline of the Atlantic Meridional Overturning Circulation. Geophysical Research Letters 47, e2019GL086075. https://doi.org/10.1029/2019GL086075

739 **Table 1: Bamboo coral location, growth metrics and reconstructed age in this study.**

Coral name	Coral ID	Genus	Seamount	Depth (m)	Lat (°N)	Lon (°E)	Calcitic section radius (mm)	Organic/ Calcitic radius ratio	Average growth rate (μm/yr)	Growth time range	Age
Car_1409m	JC094-B0132	*Acanella*	Carter	1409	9.21	-21.30	6.59	1.01	103 ± 10	1949.8 – 2013.8	64 ± 8
Kni_1985m	JC094-B0086	*Lepidisis*	Knipovich	1985	5.60	-26.97	3.46	1.23	49 ± 6	1919 – 1988	71 ± 13
Vem_1474m	JC094-B0150	*Lepidisis*	Vema	1474	10.74	-44.58	6.26	1.36	39 ± 3	1831 – 1992	161 ± 18
Vay_1455m	JC094-B0092	*Lepidisis*	Vayda	1455	14.86	-48.24	4.24	1.81	37 ± 4	1898 – 2013.8	114 ± 15

740

741

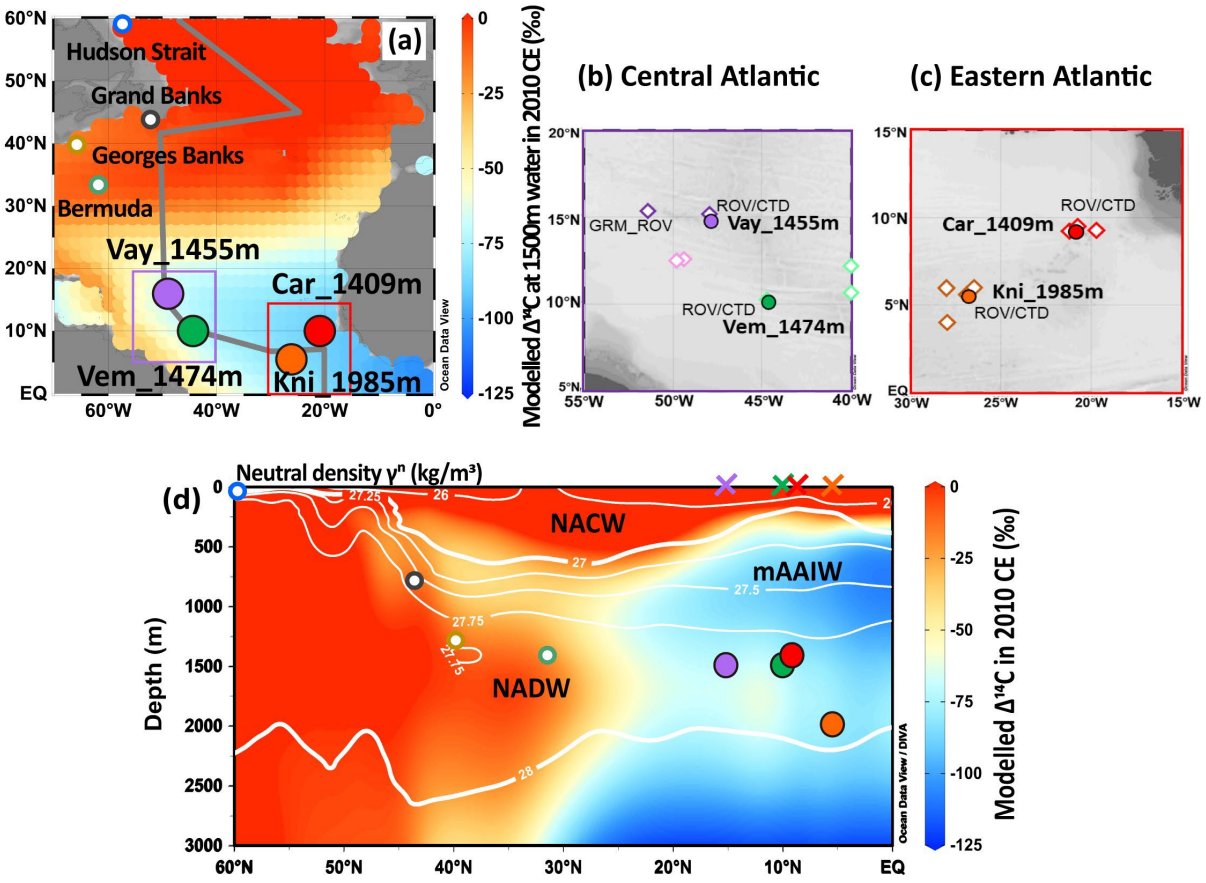

Figure 1: Map. (**a**) Bamboo coral locations in this study (filled circles) with locations of previously published $\Delta^{14}C$ records discussed in the text derived from different coral taxa (white circles with colour edges). The background of the map represents $\Delta^{14}C$ at 1500 m derived from climate-model CESM2 outputs in 2010 CE (see Section 2.5.2). The grey line represents the map section in (d). (**b** & **c**) Detailed coral locations of central and eastern Atlantic with seawater $\Delta^{14}C$ sampling locations (diamonds). Coral and seawater symbols and their colours are consistent with figures hereafter unless indicated. (**d**) Climate model CESM2 outputs of $\Delta^{14}C$ in 2010 CE along the North Atlantic (colour shading) overlain with neutral density contours obtained from GLODAPv2021. Coral symbols are consistent with (a). Cross symbols represent locations of surface $\Delta^{14}C$ records derived from organic nodes of bamboo corals in this study with their colour matched. NACW: North Atlantic Central Water; mAAIW: modified Antarctic Intermediate Water; NADW: North Atlantic Deep Water.

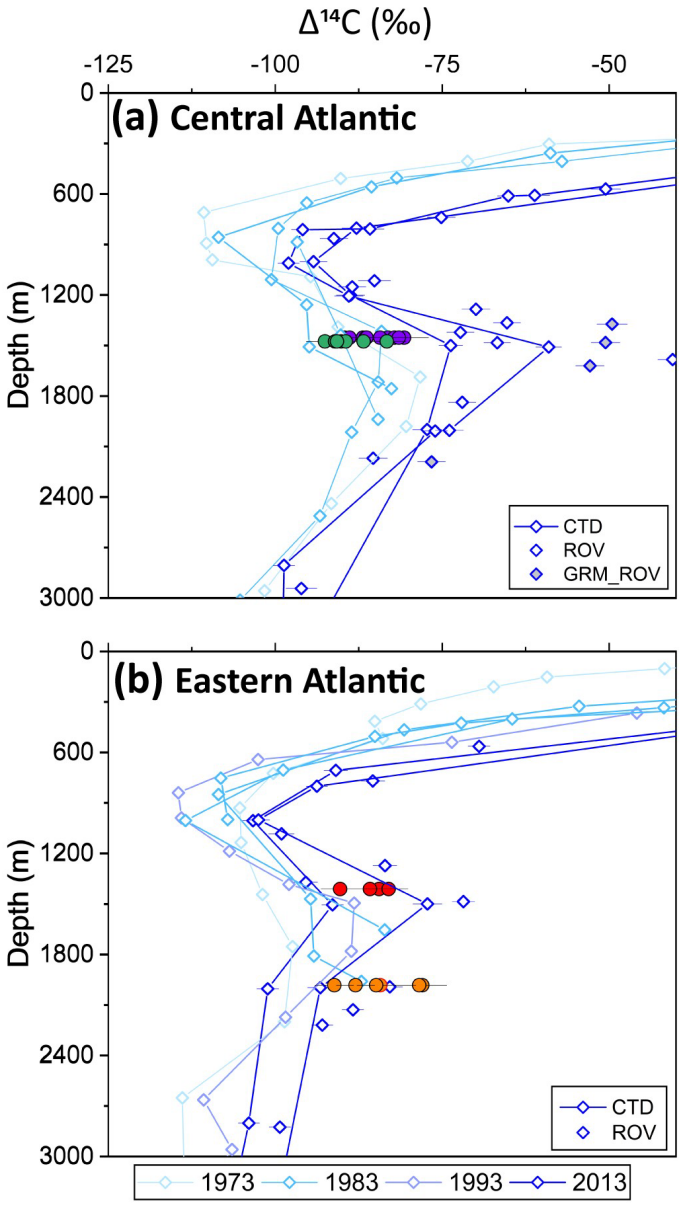

Figure 2: Seawater dissolved inorganic carbon $\Delta^{14}C$ profiles since the 1970s along with calcitic $\Delta^{14}C$ recorded in bamboo corals in this study. (**a**) Central Atlantic; (**b**) Eastern Atlantic. The symbols of calcitic $\Delta^{14}C$ are the same as in Figure 1.

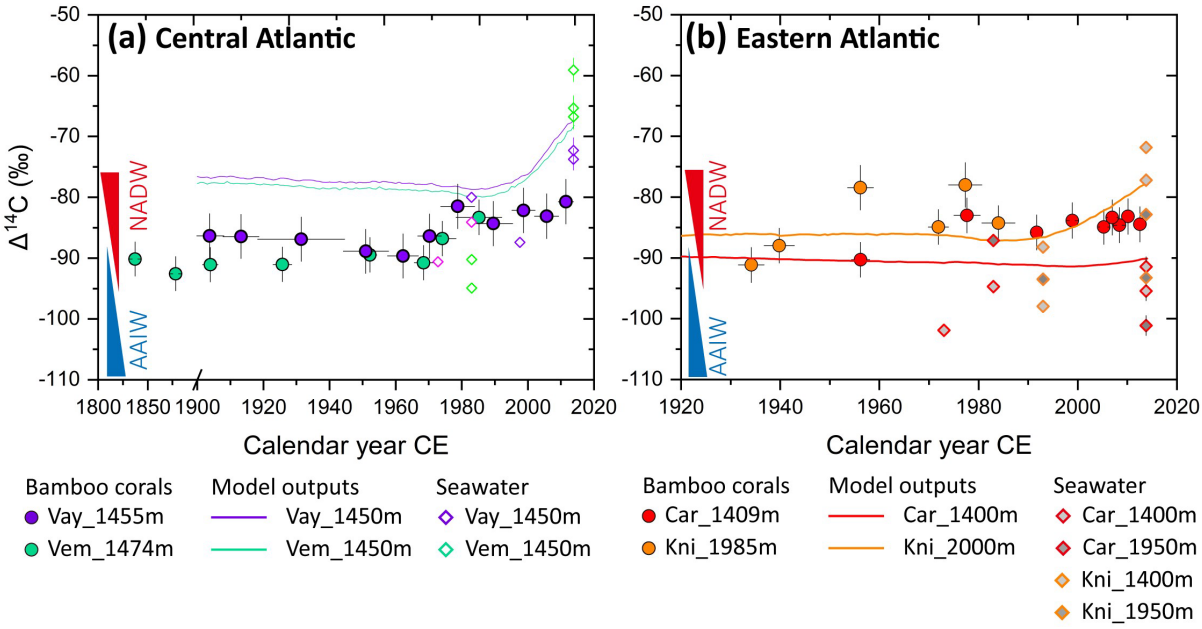

760

761 **Figure 3: $\Delta^{14}C$ records in bamboo corals calcitic skeletons compared with nearby**
762 **seawater DIC $\Delta^{14}C$ and climate model CESM2 outputs.** (**a**) Central Atlantic; (**b**) Eastern
763 Atlantic. Diamonds represent seawater DIC $\Delta^{14}C$ with edge colour matched with locations
764 shown in Figure 1b and c. Diamonds light grey and grey fill-in in (b) represent near depth to
765 coral Car_1409m and Kni_1985m, respectively. The $\boldsymbol{x}$ error bar represents the time range of
766 each subsample. The $\boldsymbol{y}$ error bar represents the 1 SD analytical error of $\Delta^{14}C$. The red and blue
767 triangles represent the range of $\Delta^{14}C$ of NADW and mAAIW in the tropical Atlantic,
768 respectively. The overlap indicates shared range of the two water masses.

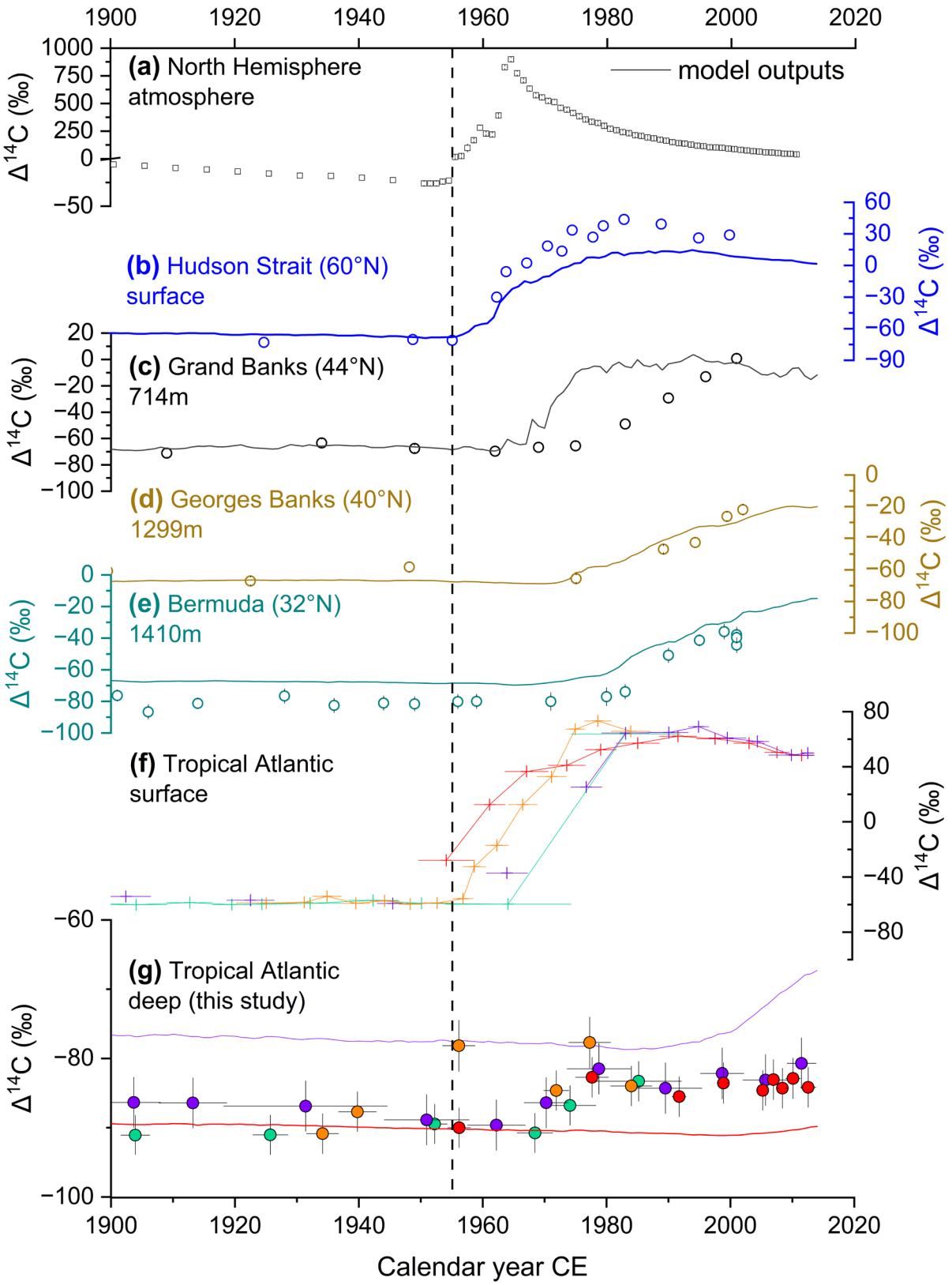

Figure 4: Radiocarbon records of (**a**) North Hemisphere atmosphere (Hua et al., 2016), (**b**) Hudson Strait cold-water gorgonian coral *Primnoa resedaeformis* organic skeleton (60°N, surface) (Sherwood et al., 2008), (**c**) Grand Banks bamboo coral calcitic skeleton (44°N, 714 m) (Sherwood et al., 2008), (**d**) Georges Banks bamboo calcitic skeleton (40°N, 1299 m)

(Farmer et al., 2015a), (**e**) Bermuda *E. rostrata* coral skeleton (32°N, 1410 m) (Lee et al., 2017), (**f**) tropical bamboo coral organic skeleton (Liu et al. 2023), (**g**) tropical bamboo corals calcitic skeleton from this study. Bamboo corals with the same colour coding from (f) and (g) are the same corals. Colour coding refers to Figure 1. Line in each plot represents $\Delta^{14}C$ record derived from climate-model outputs of corresponding location (Danabasoglu, 2019; Orr et al., 2017). The dash line denotes the response time of the atmosphere on bomb radiocarbon.

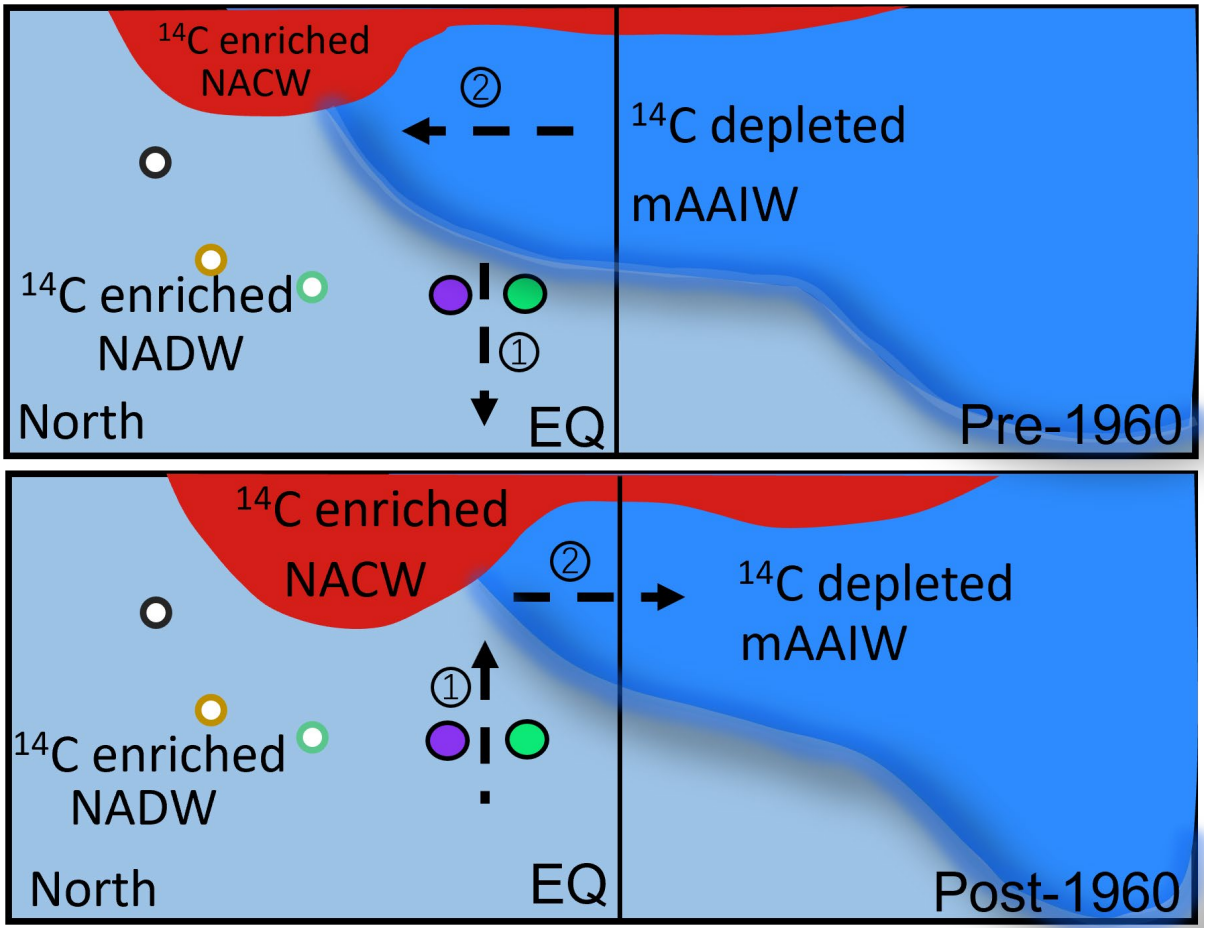

Figure 5: Schematic of potential changes in water mass after ~1960 CE. The schematic plot shows two scenarios of potential changes: (1) the expansion or shoaling of ^{14}C-enriched water mass North Atlantic Deep Water (NADW) after ~1960 CE; (2) ^{14}C depleted modified Antarctic Intermediate Water (mAAIW) retreated after ~1960 CE. These shifts could explain why coral sites became more influenced by ^{14}C enriched NADW after ~1960 CE. Coral symbols are the same as in Figure 1.

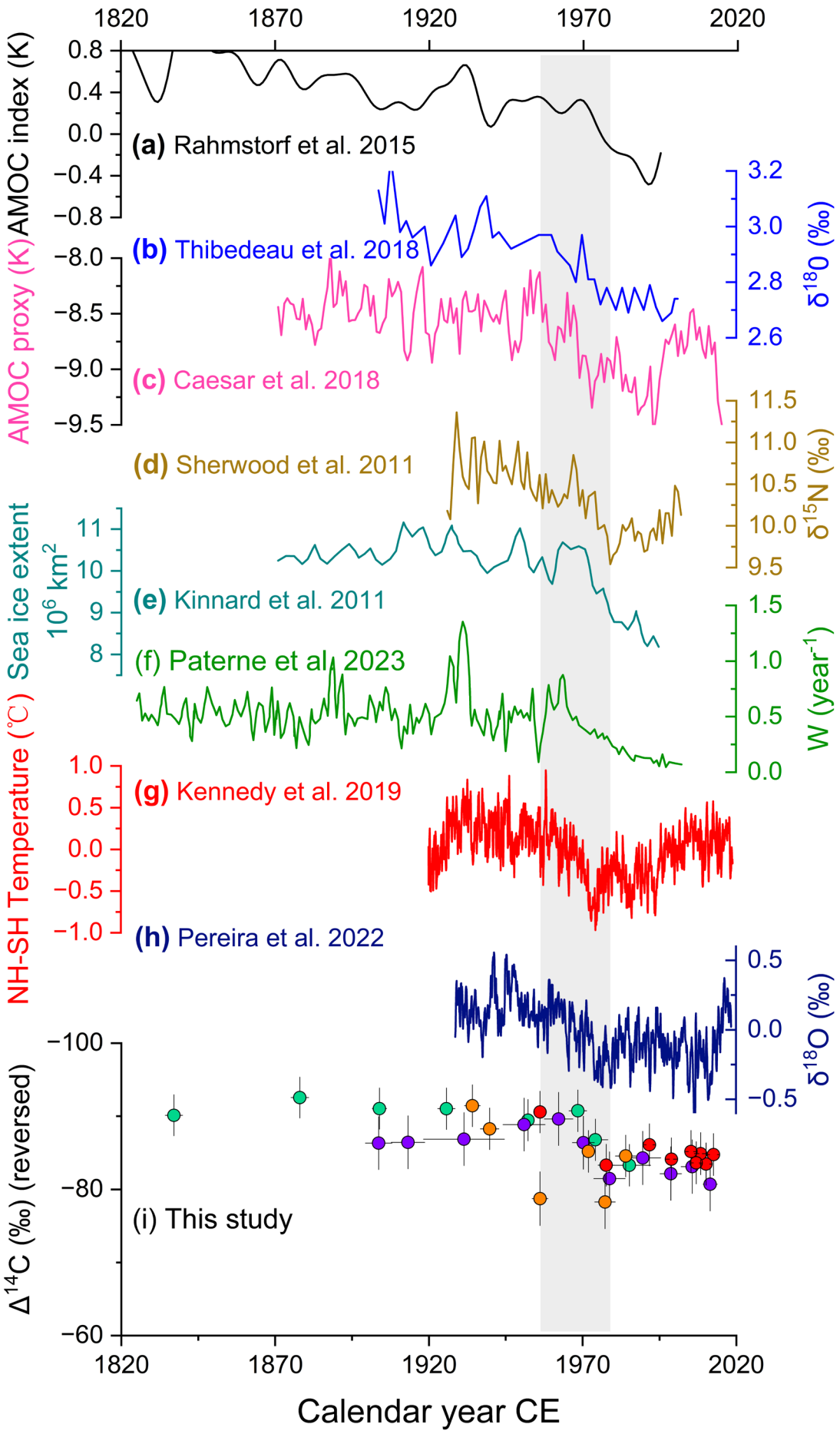
1820
1870
1920
1970
2020
AMOC index (K)
0.8
0.4
0.0
−0.4
−0.8
(a) Rahmstorf et al. 2015
AMOC proxy (K)
−8.0
−8.5
−9.0
−9.5
(b) Thibedeau et al. 2018
3.2
3.0
2.8
2.6
δ18O (‰)
(c) Caesar et al. 2018
(d) Sherwood et al. 2011
11.5
11.0
10.5
10.0
9.5
δ15N (‰)
Sea ice extent
10^6 km^2
11
10
9
8
(e) Kinnard et al. 2011
(f) Paterne et al. 2023
1.5
1.0
0.5
0.0
W (year^-1)
NH-SH Temperature (°C)
1.0
0.5
0.0
−0.5
−1.0
(g) Kennedy et al. 2019
(h) Pereira et al. 2022
0.5
0.0
−0.5
δ18O (‰)
Δ14C (‰) (reversed)
−100
−80
−60
(i) This study
1820
1870
1920
1970
2020
Calendar year CE

Figure 6: AMOC proxies comparison. (**a**) AMOC index obtained by the difference between subpolar gyre and Northern Hemisphere temperature anomalies (Rahmstorf et al., 2015); (**b**) the Laurentian Channel benthic foraminifera $\delta^{18}O$ record (Thibodeau et al., 2018); (**c**) AMOC proxy obtained by sea surface temperature anomaly in subpolar gyre region in HadISST data (Caesar et al., 2018); (**d**) bulk $\delta^{15}N$ recorded in cold-water gorgonian coral *Primnoa resedaeformis* over the Canadian shelf (Sherwood et al., 2011); (**e**) reconstructed Arctic sea ice extent (Kinnard et al., 2011); (**f**) tropical North Atlantic vertical mixing rate (Paterne et al. 2023); (**g**) Atlantic interhemispheric sea surface temperature difference from the HadISST product (Kennedy et al. 2019); (**h**) $\delta^{18}O$ record revealed from shallow water coral collected from west tropical South Atlantic (Pereira et al. 2022); (**i**) $\Delta^{14}C$ recorded in tropical North Atlantic CWC (this study; coral symbols are the same as previous figures).